

Electrocatalytic Semi-Hydrogenation of Terminal Alkynes using Ligand-Based Transfer of Protons and Electrons

Maia E. Czaikowski, Sophie W. Anferov, Alex P. Tascher, and John S. Anderson*

Department of Chemistry, University of Chicago, Chicago, Illinois 60637, United States.

ABSTRACT: Alkyne semi-hydrogenation is a broadly important transformation in chemical synthesis. Here, we introduce an electrochemical method for the selective semi-hydrogenation of terminal alkynes using a dihydrazonopyrrole Ni complex capable of storing an H₂ equivalent (2H⁺ + 2e⁻) on the ligand backbone. This method is chemoselective for the semi-hydrogenation of terminal alkynes over internal alkynes or alkenes. Mechanistic studies reveal that the transformation is concerted and Z-selective. Calculations support a ligand-based hydrogen-atom transfer pathway instead of a hydride mechanism which is commonly invoked for transition metal hydrogenation catalysts. The synthesis of proposed intermediates demonstrates that the catalytic mechanism proceeds through a reduced formally Ni(I) species. The high yields for terminal alkene products without overreduction or oligomerization are among the best reported for any homogeneous catalyst. Furthermore, the metal-ligand cooperative hydrogen transfer enabled with this system directs the efficient flow of H-atom equivalents toward alkyne reduction rather than hydrogen evolution, providing a blueprint for applying similar strategies towards a wide range of electroreductive transformations.

INTRODUCTION

The semi-hydrogenation of alkynes is an important transformation in many pharmaceutical, agrochemical, and materials applications (Figure 1).¹⁻³ This importance has spurred a great deal of research into methodologies for the selective semi-hydrogenation of alkynes, with primary goals being the prevention of overreduction to alkanes as well as controlling E/Z selectivity. Lindlar's catalyst is a classic heterogeneous example which mediates the semi-hydrogenation of internal alkynes with Z selectivity. There have also been impressive advances with homogeneous catalysts for both E and Z-selective semi-hydrogenations, as well as recent advances in using more abundant first-row transition metal catalysts.⁴⁻⁹

Despite these advances, there are several drawbacks to currently employed semi-hydrogenation technologies. Most methodologies typically operate under an H₂ atmosphere which poses flammability and pressure hazards (Figure 1). Furthermore, selectivity against overreduction to alkanes is typically dependent on steric changes upon conversion from an alkyne to an alkene. This manifests in a dearth of catalysts that are selective for the semi-hydrogenation of unprotected terminal alkynes without deleterious alkyne dimerization, overreduction, or catalyst decomposition.^{10,11} These challenges motivate the discovery of new alkyne semi-hydrogenation processes.

In thinking of alternative semi-hydrogenation protocols, and particularly in strategies that avoid the use of gaseous H₂, electrochemical transformations have many innate benefits. Electrocatalysis allows for precisely controlled redox transformations without the addition of stoichiometric chemical reductants or oxidants.¹²⁻¹⁵ The direct synthetic use of electricity can also provide a sustainable methodology when electricity is sourced renewably. These factors, coupled with the decreasing cost of renewable electricity, motivates investigations into converting classic thermal industrial and fine

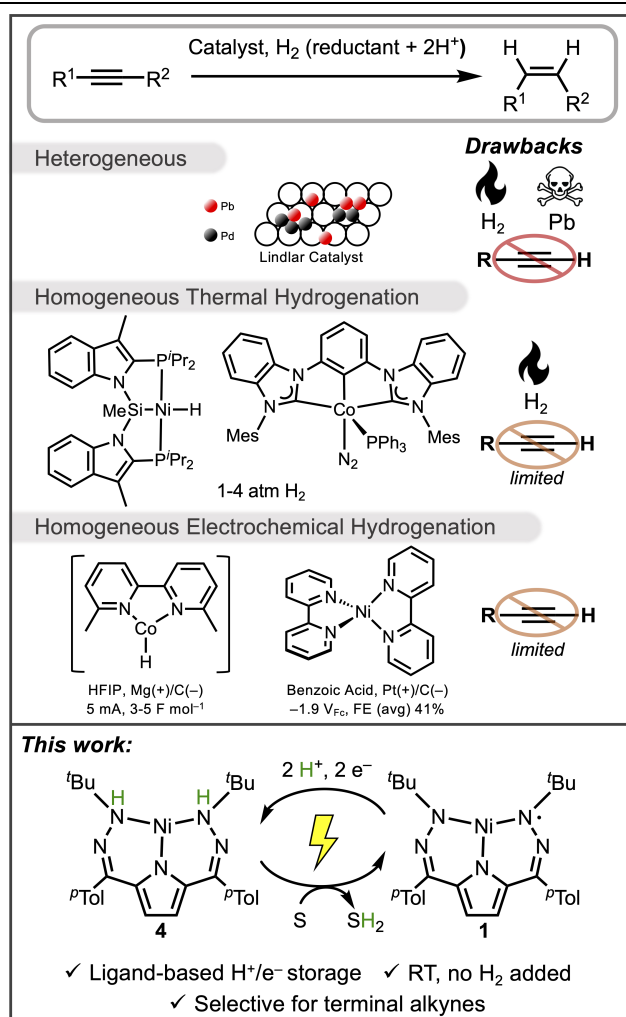


Figure 1. Overview of hydrogenation strategies including heterogeneous, homogeneous, and electrochemical systems.

chemical transformations into electrocatalytic processes.¹⁶ These attractive features have made electrocatalytic reductive transformations a burgeoning area, but homogeneous electrocatalysts are comparatively under-explored for these useful reactions.¹⁷

For alkyne semi-hydrogenation in particular, two electrocatalytic Ni and Co bipyridine complexes have shown good efficiency with internal alkynes with good to excellent Z selectivity.^{18,19} However, both of these systems suffer from poor tolerance of terminal alkyne substrates attributed to the propensity for dimerization and overreduction. Recent mechanistic investigations of the Ni bipyridine electrocatalytic system suggest a hydride-free mechanism for this transformation, which is in contrast to the prevailing mechanism for most homogeneous semi-hydrogenation catalysts involving the formation of a metal hydride which engages in alkyne reduction.^{10-14,18,20} In either mechanistic scenario, the controlled flow of H-atom equivalents is critical to turnover and selectivity.

We have been interested in utilizing ligand-based storage of H₂, or equivalently H⁺ and e⁻ equivalents, to mediate both reductive and oxidative transformations. This approach relies on storage and transfer of H-atom equivalents from the secondary coordination sphere, akin to enzymatic systems, thus enabling new strategies for achieving challenging and novel transformations.²¹⁻³¹ While several systems have demonstrated H-atom storage, examples of the ligand-based storage of a full equivalent of H₂ are more uncommon.³²⁻⁴⁶ We have specifically been investigating a dihydrazonopyrrole (DHP) ligand scaffold that can store a full equivalent of H₂ which enables catalytic thermal hydrogenations of alkenes and quinones.^{21,47} Given this reactivity, we questioned whether H₂ could be replaced by acid and an electrode and also whether the metal-ligand cooperative hydrogenation reactivity and selectivity of this system would be altered under this electrochemical regime.

Indeed, we have found that DHP Ni complexes are excellent electrocatalysts for the selective semi-hydrogenation of alkynes (Figure 1). Specifically, we see good selectivity and conversion with a broad scope of alkynes, particularly terminal alkynes, without evidence for overreduction or oligomerization. Mechanistic investigations underscore the importance of DHP ligand stored reducing equivalents, in parallel to recent observations of hydride free mechanisms.²⁰ Finally, this system displays good efficacy and scope for a variety of substrates including drug molecules and diynes. These results add to the growing body of literature demonstrating the utility of reductive electrocatalysis in providing alternative strategies to classic transformations and also demonstrate how metal-ligand cooperative strategies for H₂ or H-atom storage can enable new catalysis.

RESULTS AND DISCUSSION

Electrochemical characterization

We initially targeted the previously reported complex (^tBu, Tol)DHP)Ni(II) (**1**) as a pre-catalyst.⁴⁸ The cyclic voltammogram (CV) of **1** in acetonitrile shows two reversible redox events at peak potentials (E_{1/2}) of -0.1 and -1.1 V vs Fc^{0/+}. We assign these features to a ligand-based oxidation and reduction of the starting complex to form **1**⁺ and **1**⁻, respectively (Figure 2A). Additionally, the CV of **1** in THF

possesses a quasi-reversible reduction at -2.6 V vs Fc^{0/+} which we assign to a putative Ni(II)/(I) couple (Figure S11). To test the possibility of electrochemical hydrogenation with **1**, we initially investigated how these CV features were affected by added acid. These experiments are particularly important as parasitic H₂ evolution is likely to be competitive with any desired hydrogenation reactivity.

The first reduction feature of **1** shifts 300 mV anodically and becomes irreversible upon the addition of 10 equivalents of benzoic acid, likely due to protonation of the ligand altering the reversibility of this reduction (Figure 2B). Complex **1** also displays an electrocatalytic onset at -1.5 V vs Fc^{0/+} in the presence of benzoic acid. This onset is 500 mV less negative than the onset potential of benzoic acid on the carbon electrode surface alone. This catalytic response is due to H₂ evolution and we note that many Ni catalysts are known to be active electrocatalysts for this reaction (Figure S57).⁴⁹⁻⁶⁰

Despite the potential for H₂ evolution side reactivity, we still

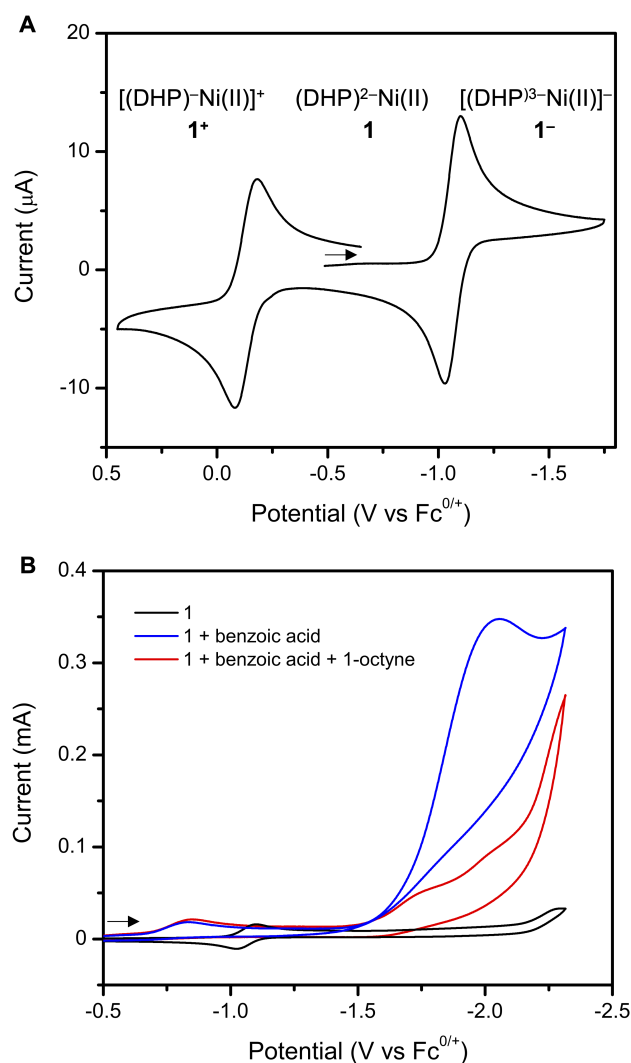


Figure 2. (A) CV of **1** (1 mM) in MeCN. 0.1 M TBAPF₆, 100 mV s⁻¹, scanning reductively. (B) CV of **1** alone, with 10 eq benzoic acid, and with 10 eq benzoic acid and 10 eq 1-octyne. 1 mM **1**, 0.1 M TBAPF₆ in MeCN, 100 mV s⁻¹, scanning reductively.

wanted to test whether the net H^+ and e^- equivalents delivered electrochemically could be harnessed for hydrogenation reactivity. Indeed, upon addition of 1-octyne, the catalytic feature at -1.5 V vs $Fe^{0/+}$ is suppressed and adopts a new waveform consistent with a change in reactivity in the presence of an alkyne substrate (Figure 2B). This suggests that the catalytically active form of **1** may selectively react with an alkyne substrate despite competing hydrogen evolution reactivity (HER). These promising initial results from CV prompted us to perform bulk electrolyses to determine the major product of alkyne reactivity and whether this catalytic system diverts H-atom equivalents from HER efficiently.

Semi-Hydrogenation Reactivity and Scope

Bulk electrolysis was carried out under constant current in a divided cell. Under standard conditions ($[Ni] = 1$ mM; $[alkyne] = 10$ mM; $[BA] = 100$ mM; $i = 4$ mA, $t = 55$ min) terminal alkyne substrates were successfully semi-hydrogenated and overreduced or oligomerized byproducts were not detected by GC/MS analysis. The semi-hydrogenated product of 1-octyne is produced in 71% chemical yield and 33% Faradaic efficiency (FE). The conversion of phenylacetylene to styrene proceeds in 96% chemical yield with a 45% FE. While the yield and FE for aliphatic terminal alkynes are somewhat lower than for phenylacetylenes, the observed conversion and yields here are among the best reported across both aryl and alkyl terminal alkynes in any homogeneous catalytic system. Control electrolyses excluding **1** or benzoic acid showed no conversion of the 1-octyne starting material. Substituting **1** with a generic Ni salt,

$Ni(MeCN)_3OTf$, resulted in a mixture of 1-octene and oligomeric products in 11% and 14% yield, respectively (Figure S58). This loss of selectivity and conversion for semi-hydrogenation with a generic Ni salt is reminiscent of the lower yields and conversion for many other catalysts for the reduction of terminal alkyne substrates, indicating an essential role for the dihydrazonopyrrole ligand in the high selectivity we observe. As a final control, post-electrolysis electrodes are inactive in fresh electrolyte without **1**. Together, these tests strongly support that the active catalyst species involves a well-defined molecular ($^{tBu,Tol}DHP$)Ni complex.

Various parameters were tuned to optimize the conditions for bulk electrolysis and maximize the yield of semi-hydrogenated products. Modifying the current showed that 4 mA produced an optimal yield with again a surprisingly good FE of 40-50% for most substrates (Table S1). Using hexafluoroisopropanol as a proton source resulted in poor yields, as did switching to THF solvent. Maximum yield and FE were achieved at 55 minutes of constant current with plateauing yields with further time (Figure S16). An RVC electrode was selected to disfavor HER, and yields improved by 10-20% compared to a graphite rod electrode. Optimized electrolyses were performed in a divided cell. While conversion also proceeds in good yield with an undivided cell, Zn^0 plating from the sacrificial Zn anode onto the RVC cathode was avoided in a divided cell.

A variety of substrates were then tested with these optimized conditions to determine the reaction scope. A broad set of functional groups were tolerated including pyridines, thiophenes, aryl chlorides, cyclopropyl, and hydroxyl groups (Figure 3). Good yields of

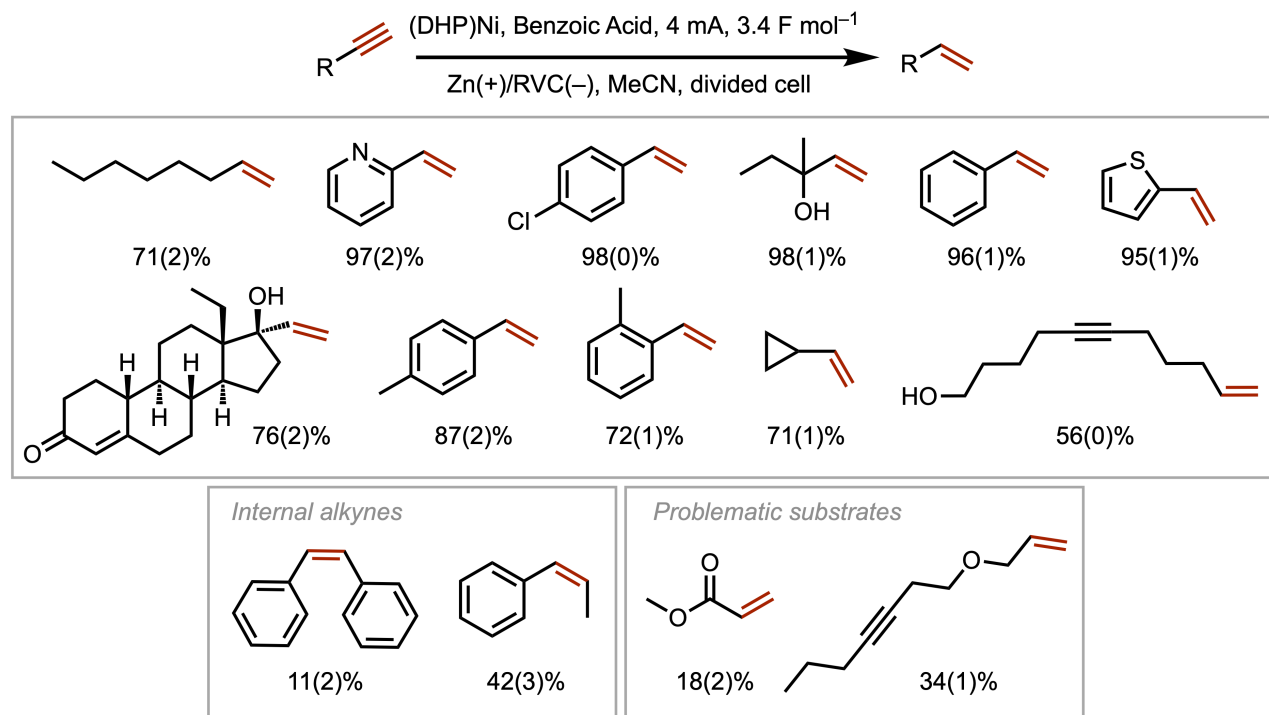


Figure 3. Substrate scope for alkyne semi-hydrogenation using 1 mM **1**, 10 mM substrate, and 100 mM benzoic acid in MeCN. 0.1 M TBAPF₆, constant current electrolysis, $t = 55$ min. Chemical yields given as a percentage with standard deviation in parentheses. $F \text{ mol}^{-1}$ calculated based on alkene under galvanostatic conditions at 4 mA.

the corresponding terminal alkene were also observed for the common drug compound levonorgestrel, which possesses a tertiary alcohol group as well as an α,β -unsaturated carbonyl. This result supports the ability of **1** to perform late-stage semi-hydrogenations of terminal alkynes in complicated molecules. Furthermore, 3.4 F mol^{-1} is passed in all cases, consistent with near-50% FE for semi-hydrogenation over hydrogen evolution for most substrates. The functional group tolerance of **1** is improved in comparison to recent Ni electrocatalysts¹⁹ and is similar to recent Co systems,¹⁸ with the notable exception of ester groups which are not well-tolerated in our case. We note that the activity of **1** for unprotected terminal alkynes is unusual for homogeneous electrocatalytic systems, with only limited activity or selectivity in previous reports.

We can also compare the activity of **1** to the limited examples of terminal alkyne thermal semi-hydrogenations using H_2 . Complex **1** has an improved scope and yield over a previously reported Mn bis(di-*iso*-propylphosphino)ethane catalyst,⁵ and comparable tolerance of chlorides, thiophenes, and methyl-substituted phenylacetylenes to an Fe N-methyl PNP pincer catalyst.⁷ We note the observation that improving the bulkiness of the PNP pincer ligand for the aforementioned Fe catalyst improved selectivity for the semi-hydrogenated terminal alkene product rather than dimerized or overreduced byproducts.⁷ Likewise, in our system we hypothesize that the bulkiness of the *t*Bu groups around the Ni center introduce steric hindrance that selects for terminal alkyne substrates over alkenes or bulkier internal alkynes. This is exemplified by the 11% yield of stilbene obtained from diphenylacetylene with **1** under the standard electrolysis conditions with the remainder of the carbon balance corresponding to unreacted starting material.

Catalytic Mechanism

The high activity and selectivity of **1** motivated us to investigate its mechanism. An important mechanistic question is whether **1** directly reduces alkynes, or whether in-situ generated H_2 enables thermal hydrogenation catalysis. However, electrolysis of **1** and 1-octyne with an atmosphere of H_2 results in <5% yield of 1-octene (Table S1). This demonstrates that any H_2 generated during electrocatalysis contributes only minimally to product formation. This finding is consistent with previous studies which showed this system is capable of activating H_2 for quinone hydrogenation, but not for alkenes.⁴⁷

The order in benzoic acid for semi-hydrogenation cannot be concretely determined by analyzing the CV due to overlapping HER (Figure 2). However, we note that the initial feature of the catalytic wave only appears when substrate is present along with acid, and that increasing benzoic acid concentration does not increase the current of this feature (Figure S15). These observations suggest that catalytic turnover is zero order in acid, which is supported by the DFT calculated rate-determining step of intramolecular HAT (*vide infra*). The addition of 1-octyne suppresses the HER wave of **1** but increasing the 1-octyne concentration beyond an equimolar amount with benzoic acid does not provide any further change in the catalytic wave (Figure S13).

We then analyzed the speciation of **1** with added acid or substrate by CV. The addition of 1-octyne to **1** without any added acid shows

no change in the reversible redox features, suggesting that **1** does not bind 1-octyne in its neutral or I^- reduced oxidation state (Figure S12). The addition of sub-stoichiometric benzoic acid to **1** without added 1-octyne induces a color change from deep purple to maroon and improved solubility in MeCN compared to the starting complex. The CV of this mixture shows a gradual diminishment of the reversible redox feature at $-1.1 \text{ V vs Fc}^{0/+}$ as two new irreversible features arise at -0.6 and $-0.9 \text{ V vs Fc}^{0/+}$ (Figure S14). Eventually, the dominant feature is a broad irreversible reduction at $-0.9 \text{ V vs Fc}^{0/+}$ after >2 equivalents of benzoic acid have been added (Figure S15). We postulate that the speciation at low concentrations of acid arises from an equilibrium between mono- and di-protonated analogues of **1**. The single irreversible feature with additional acid possibly corresponds to the reduction of a di-protonated ligand-metal complex. However, more detailed assignment of differentially protonated congeners of **1** is challenging due to the paramagnetic nature of these species.

While the product(s) of **1** and benzoic acid are paramagnetic and difficult to characterize, initial reduction of **1** with 1 eq of CoCp_2^* provides $[(^{\text{tBu,Tol}}\text{DHP})\text{Ni}]^-[\text{CoCp}_2^*]^+$ (**2**) which is diamagnetic. This enables protonation studies with NMR spectroscopy, and the addition of 2 equivalents of benzoic acid to **2** results in a color change from indigo to light yellow. We tentatively assign this new product as $[(^{\text{tBu,Tol}}\text{DHPH}_2)\text{Ni}]^+[\text{BzO}]^-$ (**3**) where the β -Ns of both hydrazone arms have been protonated. Evidence of these protonated ligand arms is provided by ^1H NMR and IR spectroscopies which show diagnostic resonances and stretches, respectively (Figures S3 and S21). Furthermore, the ^1H NMR of **3** is in agreement with the previously reported and characterized complex $(^{\text{tBu,Tol}}\text{DHPH}_2)\text{NiOTf}$.⁴⁷

Interestingly, no hydrogenated products are observed when **3** is stirred with excess 1-octyne (Figure S4). This indicates that **3** is not the active hydrogenating intermediate. The catalytic CVs for **1** support this hypothesis. The onset potential for catalysis begins nearly 0.7 V negative of the first irreversible reduction of the Ni complex in the presence of benzoic acid. We hypothesized that an additional reduction event corresponding to a formal Ni(II)/Ni(I) couple might be necessary for catalysis. Indeed, isolated $(^{\text{tBu,Tol}}\text{DHPH}_2)\text{NiOTf}$ has an irreversible reduction feature at $-1.6 \text{ V vs Fc}^{0/+}$, which is nearly superimposable with the catalytic onset of **1** in the presence of benzoic acid (Figure S18). As this complex has a reduced DHP ligand, this feature is most reasonably assigned as a Ni(II)/Ni(I) couple. The irreversibility of this feature is likely induced by a chemical change such as proton loss upon reduction. While **3** is not reactive with 1-octyne, the addition of Na/Hg amalgam as a reductant with **3** leads to the production of 1-octene in 32% yield (Figure S5). We attribute this comparatively low yield to some decomposition of complex **3** owing to the strongly reducing conditions. Stirring 1-octyne and benzoic acid with Na/Hg in the absence of **3** recovers only 1-octyne starting material. To further corroborate the presence of a Ni(I) species, compound **3** was stirred with Na/Hg amalgam followed by rapid freezing at $-78 \text{ }^\circ\text{C}$. The X-band EPR spectrum is consistent with a Ni(I) species, with a broad rhombic signal and features at $g = 2.073, 2.123, \text{ and } 2.270$ (Figure S19). The EPR spectrum is distinct from that of complex **1** which is formally Ni(II) with a

ligand radical.⁴⁸ These combined data, and particularly the need to add an additional reductant to **3** to react with alkynes, supports that a reduction to a Ni(I) species (**4**) is critical to initiating catalysis.

With evidence supporting the necessity of the two-electron reduction of **1** in the presence of acid before the system is catalytically active, we then investigated the chronoamperometry of bulk electrolyses to gain additional mechanistic insights. Specifically, we had noted a distinctive initiation period which we thought might correspond to an initial reduction of the Ni species in solution (Figure S16). Calculating the moles of electrons passed during this period corresponds with a two-electron reduction of the added catalyst (see SI). Use of (^tBu,^{Tol}DHPH₂)NiOTf instead of **1** should in principle reduce this induction period as the catalyst is already reduced. Satisfyingly, this substitution indeed shortens the initiation period and reaches a similar potential and overall yield as the standard conditions which supports the hypothesis that a Ni(I) species needs to be generated (Figure S17).

We also wanted to obtain more insight on the net H-atom transfer steps of catalysis and so we analyzed the products of the low-yielding internal alkyne substrates diphenylacetylene and 1-phenyl-1-

propyne. We found that both of these substrates gave the *Z*-isomer of the stilbene and β -methyl-styrene products, respectively (Figures S46 and S47). While no *E* products were detected for these internal alkyne substrates, deuterium labelling studies with d₁-benzoic acid and phenylacetylene revealed a 1:0.6 *Z*:*E* ratio for terminal alkyne semi-hydrogenation (Figure 4C). These observations suggest that the semi-hydrogenation proceeds in a *cis*-selective manner with some possible competition or isomerization for terminal alkyne substrates. It is possible that the smaller steric profile of terminal alkene products might favor coordination to Ni and subsequent isomerization.

As a last mechanistic test, we also investigated the possible involvement of radical intermediates such as free alkenyl radicals. We note that previous thermal hydrogenations with DHP complexes of Co do show evidence for radical intermediates.²¹ To test this possibility we employed a radical cyclization probe, allyl-2-ethynylbenzene, which might be expected to undergo a cyclization to a five-membered ring from a putative radical intermediate (Figure 4B). While this compound is unstable and undergoes some degree of polymerization in MeCN, we detected no cyclized products and

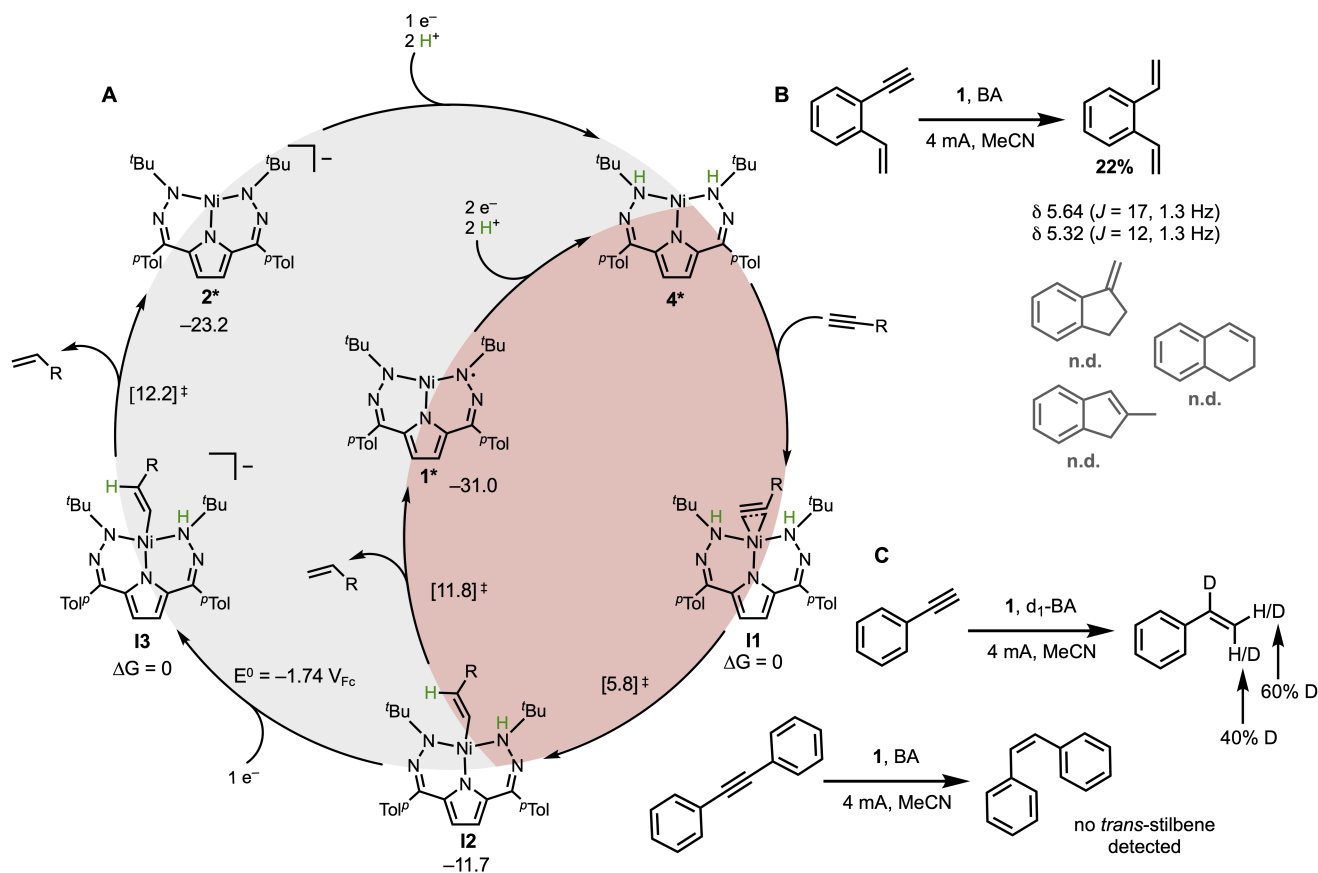


Figure 4. Mechanistic studies. (A) Proposed catalytic cycle with neutral and anionic pathways shown. DFT computed energies (kcal/mol) were carried out with the M06L functional, def2-TZVPP basis set for Ni, and def2-TZVP for all other atoms. Asterisks indicate experimentally characterized intermediates. (B) Radical probe experiment using allyl-2-ethynylbenzene and (C) deuterium incorporation experiment using d₁-benzoic acid with phenylacetylene, and semi-hydrogenation of diphenylacetylene to give 11% chemical yield of *cis*-stilbene with no *trans* product detected. Standard electrolysis conditions: [Ni] = 1 mM; [alkyne] = 10 mM; [BA] = 100 mM; [TBAPF₆] = 0.1 M; *i* = 4 mA, *t* = 55 min, MeCN, RVC/Zn.

solely the expected 1,2-divinylbenzene product which should arise from hydrogenation (Figure S8). The rate constant for cyclization for similar vinyl radical species is on the order of 10^8 s^{-1} , indicating that semi hydrogenation proceeds through a concerted mechanism without long-lived radical intermediates.⁶¹

We then employed density functional theory (DFT) computations to gain additional mechanistic insight and to fill in a complete mechanistic cycle (Figure 4A). Beginning from the fully reduced Ni(I) complex **4**, coordination to 1-butyne gives calculated bond distances of 1.969 and 2.008 Å, showing a nearly symmetrically bound alkyne. The first net H-atom transfer (HAT) has a transition state barrier of 5.8 kcal/mol and is overall exergonic by 11.7 kcal/mol. After this initial low-barrier step to form **I2**, we envisioned two plausible pathways by which the cycle could proceed. A second HAT could release the alkene product and give **1**. This path proceeds via a ~23 kcal/mol transition state barrier for an overall 19 kcal/mol downhill process. If instead the alkenyl adduct is first reduced by one electron to generate **I3**, the subsequent transition state barrier for HAT is 12.2 kcal/mol for an overall 23.2 exergonic process. Both pathways regenerate the starting species **4** by subsequent reduction and protonation. The lower transition state barrier for the second HAT step, along with the accessible calculated reduction potential of -1.74 V vs $\text{Fc}^{0/+}$ in MeCN, supports initial reduction to an anionic alkenyl intermediate as the most plausible of the two calculated cycles.

One interesting feature of this proposed cycle is the lack of any metal-hydride intermediates. To further test this observation, we computationally explored the feasibility of a Ni hydride species via reduction and migration of one proton from the ligand. The formation of a (DHP)Ni-H species is calculated to be slightly endergonic, and the resultant coordinatively saturated hydride species is not computed to have favorable alkyne binding (Table S14). We also note that we have seen no evidence by either ^1H NMR or IR spectroscopy that would indicate the presence of a hydride species, but we do observe ligand-based proton storage for **3** which is the precursor to the proposed catalytically active complex **4** (Figures S3 and S21). These data suggest that ligand-based secondary coordination sphere reactivity is the most viable pathway. This hydride-free pathway echoes recent mechanistic proposals from Leitner and co-workers where an ECEC semi-hydrogenation pathway with a nickelacyclopropene adduct resting state was invoked.²⁰ This system uses a bipyridine ligand and relied on direct outer sphere protonation to a reduced metallacyclopropene intermediate followed by rapid electron transfer. In contrast, both experimental and computational evidence supports a more concerted H-atom transfer in the present system. The DFT-calculated BDE for the DHP N-H bond of 56 kcal/mol is comparatively small and thus energetically accessible for an HAT pathway (Table S12). Inspection of the Mulliken charges along the reaction coordinate also suggests that each transition state is best described as an H-atom ($\text{H}^+ + \text{e}^-$) transfer rather than a heterolytic proton and hydride transfer (Table S13). Thus, while both of these Ni based electrocatalysts rely on hydride free mechanisms, the present DHP system leverages secondary-coordination sphere interactions to specifically shuttle H-atom equivalents to the bound alkyne

substrate as opposed to more purely outer-sphere steps in the bipyridine system.

CONCLUSION

We describe a homogeneous electrocatalytic system for the semi-hydrogenation of terminal alkynes and corresponding mechanistic investigations which support a ligand-assisted mechanism and Z-selective hydrogenation. The $(^{\text{tBu,Tol}}\text{DHP})\text{Ni}$ complex catalyzes selective semi-hydrogenation of a variety of alkyne substrates including those with alcohol, thiophene, pyridine, cyclopropyl, and chloride functional groups. The selective semi-hydrogenation of terminal alkynes without significant oligomerization or overreduction is unusual generally, and particularly so for an electrochemical system.

Mechanistic investigations support the importance of HAT from ligand-stored H-atom equivalents to Ni coordinated alkyne substrates. In our proposed catalytic pathway, the ligand and metal center work in tandem to selectively shuttle protons and electrons in a coordinated manner. While most examples of hydrogenation catalysts employ a metal hydride mechanism, this DHP system is unique in its involvement of the secondary coordination sphere, drawing inspiration from enzymatic processes. This catalytic design strategy, particularly as employed in reductive electrocatalysis here, opens new possibilities for selective and efficient transformations. Specifically, the use of electrochemical hydrogenation schemes enables fine tuning of parameters including reduction potential and acid pK_a , potentially offering more delicate control compared to chemical redox conditions. The utility of the DHP scaffold in avoiding competitive HER offers promise for general application in various reductive processes that more typically rely upon H_2 .

EXPERIMENTAL SECTION

General Considerations. All reagents were purchased from commercial suppliers and used without further purification unless otherwise specified. Complex **1** was synthesized following a previously reported procedure.⁴⁸ All manipulations were carried out under an atmosphere of N_2 using standard Schlenk and glovebox techniques. Glassware was dried at $180 \text{ }^\circ\text{C}$ for a minimum of 2 h and cooled under vacuum prior to use. Solvents were dried on a solvent purification system from Pure Process Technology, passed over a column of activated alumina, and stored over 4 Å molecular sieves under N_2 . Tetrahydrofuran was stirred over NaK alloy and run through an additional activated alumina column prior to use to ensure dryness. C_6D_6 and CD_3CN were stored over 4 Å molecular sieves under N_2 . Solvents were tested for H_2O and O_2 using a standard solution of sodium-benzophenone ketyl radical anion. Tetrabutylammonium hexafluorophosphate and benzoic acid were dried under vacuum at $100 \text{ }^\circ\text{C}$ over 8 hours.

^1H and ^{13}C NMR spectra were recorded on a Bruker DRX 400 MHz spectrometer. Chemical shifts are reported in ppm units referenced to residual solvent resonances for ^1H spectra. Infrared spectra were recorded using a Bruker Tensor II spectrometer with OPUS software suite. IR samples were prepared using a solution cell with

KBr windows. EPR spectra were recorded on an Elexsys E500 spectrometer with an Oxford ESR 900 X-band cryostat and a Bruker Cold-Edge Stinger and were simulated using the Easyspin suite in Matlab software.⁶² GC/MS data was collected on an Agilent SQ GCMS with 5977A single quad MS and 7890B GC. Elemental analysis was performed by Midwest Microlabs. Electrochemical measurements were performed using a BAS Epsilon potentiostat and analyzed using BAS Epsilon software version 1.40.67NT.

Electrochemical experiments. Experiments were performed inside the glovebox with a MeCN/0.1 M *n*Bu₄NPF₆ electrolyte solution at room temperature. Cyclic voltammetry measurements were made with a [Ni] = 1 mM using a glassy carbon working electrode, platinum wire counter electrode, and silver wire pseudoreference electrode and were referenced to internal Fc/Fc⁺ by adding ferrocene at the end of measurements. A one-compartment glass cell was filled with 4 mL of electrolyte solution. The working electrode was polished over a microcloth pad (Buehler) using alumina slurry (0.05mm EMS), followed by rinsing with deionized water and isopropyl alcohol. Reference and counter electrodes were rinsed with acetone. CVs were recorded at a scan rate of 100 mV/s scanning reductively.

Electrolyses were performed in a H-type glass cell with anode and cathode chambers separated by a glass frit. An RVC (reticulated vitreous carbon, ERG Duocel, 2 cm x 0.5 cm x 0.5 cm) electrode, Zn rod (National Bureau of Standards, 3 cm x 0.5 cm x 0.5 cm), and a AgBF₄/Ag electrode (BASi, 0.05 mm, 10 mM AgBF₄ solution in MeCN 0.1 M *n*Bu₄NPF₆) were used as working, counter, and reference electrodes, respectively. To each chamber of the H-cell was added 4 mL of electrolyte solution and stir bars. Typically, 2 mg of (DHP)Ni (final concentration 1 mM), 100 mL of a mesitylene (internal standard) solution in MeCN (final concentration of 10 mM), 100 mL of a substrate solution in MeCN (final concentration of 10 mM), and benzoic acid (final concentration 1 M) were added to the cathodic chamber. Electrolyses were performed under galvanostatic conditions and aliquots were taken and diluted in MeCN before analysis by gas chromatography (GC). For determining final yield, the electrolyte solution was passed through an alumina pad and 200 mL of CD₃CN was added to 200 mL of electrolyte solution and analyzed by ¹H NMR using a mesitylene internal standard (10 mM, δ 6.77 ppm, 3H) and a solvent suppression pulse sequence. All electrolyses were performed in triplicate. For substrates with < 95% yield of the semi-hydrogenated product, GC-MS chromatograms and mass spectra are provided to check for the presence of alkene or dimerized products (See SI). Cyclopropylacetylene and methyl propiolate were too low-boiling to detect over trace solvents by GC-MS on our instrument. Potentials reported for chronopotentiometry electrolysis experiments are referenced to Fc/Fc⁺ by external measurement in an independent cell versus the AgBF₄/Ag electrode of E_{1/2}(Fc/Fc⁺) = 0.48 V vs AgBF₄/Ag. For electrolysis under an H₂ atmosphere, the cathodic chamber was prepared in an N₂ glovebox, removed from the glovebox, and sparged with H₂ for 10 min before

starting electrolysis, and then constantly during electrolysis.

X-ray structure determination. The diffraction data for **2** were measured at 100 K on a Bruker D8 fixed-chi with PILATUS1M (CdTe) pixel array detector (synchrotron radiation, λ = 0.41328 Å (30 keV)) at the Chem-MatCARS 15-ID-B beamline at the Advanced Photon Source (Argonne National Laboratory). Data reduction and integration were performed with the Bruker APEX3 software package (Bruker AXS, version 2017.3-0, 2018). Data were scaled and corrected for absorption effects using the multiscan procedure as implemented in SADABS (Bruker AXS, version 2014/5).⁶³ The structures were solved by SHELXT (Version 2014/5)⁶⁴ and refined by a full-matrix least-squares procedure using OLEX2 (XL refinement program version 2018/1).^{65,66} Structure solutions were performed with the use of standard restraints and constraints as implemented in ShelXL. We note the structure of **2** has A level CheckCIF alerts arising from the fact that this data set was collected on a synchrotron, resulting in somewhat limited data completeness. Additional crystallographic and refinement data can be found in the SI.

Synthesis of (^tBu,Tol)DHP)Ni[CoCp₂⁺] (2**).** A solution of decamethyl-cobaltocene (CoCp₂⁺, 20 mg, 0.06 mmol) in THF (1 mL) was added all at once to a stirring solution of **1** (30 mg, 0.06 mmol) in THF (2 mL). After stirring at room temperature for 2 hours, the color of the reaction mixture changed from deep violet to deep indigo. The solution was filtered, and the solvent was removed under vacuum resulting in a deep indigo solid. The product was purified by recrystallization (concentrated THF, -35°C). Yield: 44 mg, 0.053 mmol, 88%. ¹H NMR (400 MHz, C₆D₆): δ = 7.5 (d, 4H, J = 7.4 Hz), 7.08 (d, 4H, J = 7.0 Hz), 5.86 (s, 2H), 2.33 (s, 6H), 1.25 (s, 18H), 1.7 (s, 30H). ¹³C{¹H} NMR (125 MHz, C₆D₆): δ 141.7, 142.3, 138.1, 136.0, 129.3, 128.4, 111.5, 94.9, 52.7, 29.3, 20.9, 7.5. IR (ATR, cm⁻¹): 2954 (m), 2911 (m), 1511 (m, C=N), 1371 (m), 1341 (s), 1197 (m), 1103 (m), 1013 (s), 882 (w), 823 (s, C=C of CoCp₂⁺), 681 (m), 589 (m), 442 (m). Anal. Calc.: C, 69.57; H, 7.78; N, 8.45; Found: C, 69.13; H, 7.57; N, 8.25. HRA-MS (*m/z*) [M]⁺ C₄₈H₆₄N₃CoNi: 827.385 Found: 827.383.

Synthesis of (^tBu,Tol)DHPH₂)Ni(C₆H₅COO⁻) (3**).** To a stirring solution of **2** (10 mg, 0.012 mmol) at room temperature in a glovebox under N₂ atmosphere in CD₃CN (300 mL) was added benzoic acid (2.9 mg, 0.024 mmol) dissolved in CD₃CN (300 mL). After stirring for 15 minutes, the solution was transferred to an NMR tube. ¹H NMR (400 MHz, C₆D₆): δ = 7.34 (d, 4H, J = 7.3 Hz), 7.08 (d, 4H, J = 7.1 Hz), 6.49 (s, 2H), 6.20 (s, 2H), 2.26 (s, 6H), 1.16 (s, 18H). IR (solution cell, THF, cm⁻¹): 3250 (b, N-H). This compound is not sufficiently stable for further isolation.

Chemical reduction of 1-octyne with **3 and Na/Hg.** To a stirring solution of **3** (7.5 mg, 0.012 mmol) at room temperature in a glovebox under N₂ atmosphere in CD₃CN (600 mL) was added 1-octyne (17

mL, 0.12 mmol) and Na/Hg amalgam (30% Na, 10 mg). After stirring for 30 minutes, the solution was filtered to remove the amalgam and transferred to an NMR tube to look for the presence of 1-octene by ^1H NMR. The control reaction was performed under the same conditions except for the absence of **3** in solution. See Supporting Information.

Synthesis of d_1 -benzoic acid. Benzoic acid anhydride (Sigma Aldrich, 1.0 g, 4.4 mmol) was stirred in D_2O (Cambridge Isotope, 99.9%, 10 mL) and refluxed under N_2 for 48 hr. Upon cooling to room temperature, the product began to crystallize and could be collected by filtration as a white solid. The solid was further dried and purified by sublimation at 100°C under reduced pressure before use. The ^1H NMR spectrum is consistent with benzoic acid with the absence of a broad OH peak usually found at 11.5 ppm. Comparison with the ^1H NMR spectrum of benzoic acid anhydride shows that no starting material remains. See Figure S6 for overlaid spectra.

Synthesis of 1-(prop-2-yn-1-yloxy)hept-3-yne. To a stirred solution of 3-heptyn-1-ol (1.5 g, 13.4 mmol) in DMF (60 mL) K_2CO_3 (7.40 g, 53.6 mmol) was added in one portion. The resulting mixture was heated at 70°C for 0.5 h, then 3-bromo-1-propyne (1.9 g, 16.1 mmol) dissolved in DMF (40 mL) was added slowly over 5 min. The mixture was heated at 70°C for another 48 h. Upon completion, 15 mL of water was added. The mixture was extracted with Et_2O (3 x 100 mL). The combined organic layers were washed with water (4 x 100 mL) and brine (100 mL). After removal of the solvent under reduced pressure, the resulting yellow oil was purified by flash chromatography on silica gel (Hexanes/AcOEt : 95/5). Yield 96 mg (0.64 mmol, 5%). ^1H NMR (400 MHz, CDCl_3 , RT): δ = 4.73 (d, 2H, J = 2.4 Hz), 4.23 (t, 2H, J = 7.1 Hz), 2.55 (tt, 2H, J = 2.4 Hz), 2.52 (t, 1H, J = 2.4 Hz), 2.11 (tt, 2H, J = 2.4 Hz), 1.50 (m, 2H, J = 7.2 Hz), 0.96 (t, 3H, J = 7.4 Hz). ^{13}C $\{^1\text{H}\}$ NMR (125 MHz, CDCl_3 , RT): δ = 154.4, 82.4, 75.7, 74.8, 66.7, 55.3, 22.2, 20.7, 19.3, 13.4

Computational Methodology. Intermediates and transition states for the reaction coordinate with 1-butyne were optimized in ORCA⁶⁷ using the M06L functional and def2-TZVPP basis set on Ni, def2-TZVP basis set on all other atoms. Frequency calculations were performed to confirm the structures are at local minima on the potential energy surface. The calculated BDE for the ligand NH's was determined using free energies from frequency calculations with the M06L functional and def2-TZVPP basis set for Ni, def2-TZVP for all other atoms. A simplified ligand with *i*Pr groups in the place of the *p*-tol substituents were utilized as well as a 1-butyne substrate to reduce the number of atoms per calculation.

ASSOCIATED CONTENT


Supporting Information

Experimental procedures, NMR, GC/MS, electrochemistry, EPR, electrochemistry, SXRD data, and DFT (PDF)


X-ray crystallographic data for **2** (CIF)


AUTHOR INFORMATION

Corresponding Author

John S. Anderson – Department of Chemistry, University of Chicago, Chicago, Illinois 60637, United States;  orcid.org/0000-0002-0730-3018; Email: jsanderson@uchicago.edu

Authors

Maia E. Czaikowski – Department of Chemistry, University of Chicago, Chicago, Illinois 60637, United States;  orcid.org/0000-0002-1334-8140

Sophie W. Anferov – Department of Chemistry, University of Chicago, Chicago, Illinois 60637, United States.  orcid.org/0000-0003-3972-5845

Alex P. Tascher – Department of Chemistry, University of Chicago, Chicago, Illinois 60637, United States  orcid.org/0009-0006-4473-2571

Notes

The authors declare no competing financial interest.

ACKNOWLEDGMENT

This work was supported by the National Institutes of Health (R35 GM133470) and as part of the Inorganometallic Catalysis Design Center, an Energy Frontier Research Center funded by the U.S. Department of Energy, Office of Science, Basic Energy Sciences (DE-SC0012702). We thank the University of Chicago for funding, and the Sloan Foundation for a Research Fellowship to J.S.A. (FG-2019-11497). We thank Joseph Schneider for assistance with EPR measurements. We also thank the Research Computing Cluster at the University of Chicago for providing computing resources. Some data reported here was collected at ChemMatCARS Sector 15 which is supported by the NSF under grant number NSF/CHE-1834750. This research used resources of the APS, a U.S. DOE Office of Science User Facility operated for the DOE Office of Science by Argonne National Laboratory under Contract No. DE-AC02-06CH11357. We would like to thank Dr. Yu-Sheng Chen for assistance with SXRD acquisition at 15-ID-B,C,D.

REFERENCES

1. Swamy, K. C. K.; Reddy, A. S.; Sandeep, K.; Kalyani, A., Advances in chemoselective and/or stereoselective semihydrogenation of alkynes. *Tet. Lett.* **2018**, *59*, 419-429. DOI: 10.1016/j.tetlet.2017.12.057
2. Decker, D.; Drexler, H.-J.; Heller, D.; Beweries, T., Homogeneous catalytic transfer semihydrogenation of alkynes – an overview of hydrogen sources, catalysts and reaction mechanisms. *Catal. Sci. & Tech.* **2020**, *10*, 6449-6463. DOI: 10.1039/D0CY01276A
3. Li, X.-T.; Chen, L.; Shang, C.; Liu, Z.-P., Selectivity control in alkyne semihydrogenation: Recent experimental and theoretical progress. *Chinese J. Catal.* **2022**, *43*, 1991-2000. DOI: 10.1016/S1872-2067(21)64036-6
4. Lindlar, H., Ein neuer Katalysator für selektive Hydrierungen. *Helv. Chim. Acta* **1952**, *35*, 446-450. DOI: 10.1002/hlca.19520350205
5. Farrar-Tobar, R. A.; Weber, S.; Csendes, Z.; Ammaturo, A.; Fleissner, S.; Hoffmann, H.; Veiros, L. F.; Kirchner, K., E-Selective Manganese-Catalyzed Semihydrogenation of Alkynes with H₂ Directly Employed or In Situ-Generated. *ACS Catal.* **2022**, *12*, 2253-2260. DOI: 10.1021/acscatal.1c06022
6. Tokmic, K.; Fout, A. R., Alkyne Semihydrogenation with a Well-Defined Nonclassical Co–H₂ Catalyst: A H₂ Spin on Isomerization and E-Selectivity. *J. Am. Chem. Soc.* **2016**, *138*, 13700-13705. DOI: 10.1021/jacs.6b08128
7. Gorgas, N.; Brünig, J.; Stöger, B.; Vanicek, S.; Tilset, M.; Veiros, L. F.; Kirchner, K., Efficient Z-Selective Semihydrogenation of Internal Alkynes Catalyzed by Cationic Iron(II) Hydride Complexes. *J. Am. Chem. Soc.* **2019**, *141*, 17452-17458. DOI: 10.1021/jacs.9b09907
8. Hale, D. J.; Ferguson, M. J.; Turculet, L., (PSiP)Ni-Catalyzed (E)-Selective Semihydrogenation of Alkynes with Molecular Hydrogen. *ACS Catal.* **2022**, *12*, 146-155. DOI: 10.1021/acscatal.1c04537
9. Kaicharla, T.; Zimmermann, B. M.; Oestreich, M.; Teichert, J. F., Using alcohols as simple H₂-equivalents for copper-catalyzed transfer semihydrogenations of alkynes. *Chem. Comm.* **2019**, *55*, 13410-13413. DOI: 10.1039/C9CC06637C
10. Wang, S.; Uwakwe, K.; Yu, L.; Ye, J.; Zhu, Y.; Hu, J.; Chen, R.; Zhang, Z.; Zhou, Z.; Li, J.; Xie, Z.; Deng, D., Highly efficient ethylene production via electrocatalytic hydrogenation of acetylene under mild conditions. *Nature Commun.* **2021**, *12*, 7072. DOI: 10.1038/s41467-021-27372-8
11. Li, H.; Gao, Y.; Wu, Y.; Liu, C.; Cheng, C.; Chen, F.; Shi, Y.; Zhang, B., σ -Alkynyl Adsorption Enables Electrocatalytic Semihydrogenation of Terminal Alkynes with Easy-Reducible/Passivated Groups over Amorphous PdSx Nanocapsules. *J. Am. Chem. Soc.* **2022**, *144*, 19456-19465. DOI: 10.1021/jacs.2c07742
12. Yan, M.; Kawamata, Y.; Baran, P. S., Synthetic Organic Electrochemical Methods Since 2000: On the Verge of a Renaissance. *Chem. Rev.* **2017**, *117*, 13230-13319.
13. Wiebe, A.; Gieshoff, T.; Möhle, S.; Rodrigo, E.; Zirbes, M.; Waldvogel, S. R., Electrifying Organic Synthesis. *Angew. Chem. Int. Ed.* **2018**, *57*, 5594-5619.
14. Jutand, A., Contribution of Electrochemistry to Organometallic Catalysis. *Chem. Rev.* **2008**, *108*, 2300-2347.
15. Francke, R.; Little, R. D., Redox catalysis in organic electrosynthesis: basic principles and recent developments. *Chem. Soc. Rev.* **2014**, *43*, 2492-2521.
16. IRENA (2021), Renewable Power Generation Costs in 2020, International Renewable Energy Agency, Abu Dhabi.
17. Zhang, S.; Findlater, M., Electrochemically Driven Hydrogen Atom Transfer Catalysis: A Tool for C(sp³)/Si–H Functionalization and Hydrofunctionalization of Alkenes. *ACS Catal.* **2023**, *13*, 8731-8751. DOI: 10.1021/acscatal.3c01221
18. Gnaïm, S.; Bauer, A.; Zhang, H.-J.; Chen, L.; Gannett, C.; Malapit, C. A.; Hill, D. E.; Vogt, D.; Tang, T.; Daley, R. A.; Hao, W.; Zeng, R.; Quertenmont, M.; Beck, W. D.; Kandahari, E.; Vantourout, J. C.; Echeverria, P.-G.; Abruna, H. D.; Blackmond, D. G.; Minter, S. D.; Reisman, S. E.; Sigman, M. S.; Baran, P. S., Cobalt-electrocatalytic HAT for functionalization of unsaturated C–C bonds. *Nature* **2022**, *605*, 687-695. DOI: 10.1038/s41586-022-04595-3
19. Lee, M.-Y.; Kahl, C.; Kaeffer, N.; Leitner, W., Electrocatalytic Semihydrogenation of Alkynes with [Ni(bpy)₃]²⁺. *JACS Au* **2022**, *2*, 573-578. DOI: 10.1021/jacsau.1c00574
20. Durin, G.; Lee, M.-Y.; Pogany, M. A.; Weyhermüller, T.; Kaeffer, N.; Leitner, W., Hydride-Free Hydrogenation: Unraveling the Mechanism of Electrocatalytic Alkyne Semihydrogenation by Nickel–Bipyridine Complexes. *J. Am. Chem. Soc.* **2023**, *145*, 17103-17111.
21. Anferov, S. W.; Filatov, A. S.; Anderson, J. S., Cobalt-Catalyzed Hydrogenation Reactions Enabled by Ligand-Based Storage of Dihydrogen. *ACS Catal.* **2022**, *12*, 9933-9943.
22. Käß, M.; Friedrich, A.; Drees, M.; Schneider, S. Ruthenium Complexes with Cooperative PNP Ligands: Bifunctional Catalysts for the Dehydrogenation of Ammonia–Borane. *Angew. Chem., Int. Ed.* **2009**, *48*, 905–907, DOI: 10.1002/anie.200805108
23. Khaskin, E.; Iron, M. A.; Shimon, L. J. W.; Zhang, J.; Milstein, D. N–H activation of amines and ammonia by Ru via metal–ligand

- cooperation. *J. Am. Chem. Soc.* **2010**, *132*, 8542, DOI: 10.1021/ja103130u
24. Feller, M.; Diskin-Posner, Y.; Shimon, L. J. W.; Ben-Ari, E.; Milstein, D. N–H Activation by Rh (I) via Metal–Ligand Cooperation. *Organometallics* **2012**, *31*, 4083, DOI: 10.1021/om300248r
25. He, L. P.; Chen, T.; Gong, D.; Lai, Z.; Huang, K. W. Enhanced reactivities toward amines by introducing an imine arm to the pincer ligand: direct coupling of two amines to form an imine without oxidant. *Organometallics* **2012**, *31*, 5208, DOI: 10.1021/om300422v
26. Rodríguez-Lugo, R. E.; Trincado, M.; Vogt, M.; Tewes, F.; Santiso-Quinones, G.; Grützmacher, H. A homogeneous transition metal complex for clean hydrogen production from methanol–water mixtures. *Nat. Chem.* **2013**, *5*, 342– 347, DOI: 10.1038/nchem.1595
27. Myers, T. W.; Berben, L. A. Aluminum–ligand cooperative N–H bond activation and an example of dehydrogenative coupling. *J. Am. Chem. Soc.* **2013**, *135*, 9988– 9990, DOI: 10.1021/ja4032874
28. Xu, R.; Chakraborty, S.; Bellows, S. M.; Yuan, H.; Cundari, T. R.; Jones, W. D. Iron-Catalyzed Homogeneous Hydrogenation of Alkenes under Mild Conditions by a Stepwise, Bifunctional Mechanism. *ACS Catal.* **2016**, *6*, 2127– 2135, DOI: 10.1021/acscatal.5b02674
29. Sherbow, T. J.; Fettingner, J. C.; Berben, L. A. Control of Ligand pKa Values Tunes the Electrocatalytic Dihydrogen Evolution Mechanism in a Redox-Active Aluminum(III) Complex. *Inorg. Chem.* **2017**, *56*, 8651– 8660, DOI: 10.1021/acs.inorgchem.7b00230
30. Rajabimoghadam, K.; Darwish, Y.; Bashir, Y.; Pirman, D.; Eichelberger, S.; Sieler, M. A.; Swart, M.; Garcia-Bosch, I. Catalytic aerobic oxidation of alcohols by copper complexes bearing redox-active ligands with tunable H-bonding groups. *J. Am. Chem. Soc.* **2018**, *140*, 16625– 16634, DOI: 10.1021/jacs.8b08748
31. Sinha, S.; Das, S.; Mondal, R.; Mandal, S.; Paul, N. D. Cobalt complexes of redox noninnocent azo-aromatic pincers. Isolation, characterization, and application as catalysts for the synthesis of quinazolin-4(3H)-ones. *Dalton Trans.* **2020**, *49*, 8448– 8459, DOI: 10.1039/D0DT00394H
32. Thompson, E. J.; Berben, L. A. Electrocatalytic Hydrogen Production by an Aluminum (III) Complex: Ligand-Based Proton and Electron Transfer. *Angew. Chem., Int. Ed.* **2015**, *54*, 11642– 11646, DOI: 10.1002/anie.201503935
33. Margulieux, G. W.; Bezdek, M. J.; Turner, Z. R.; Chirik, P. J. Ammonia Activation, H₂ Evolution and Nitride Formation from a Molybdenum Complex with a Chemically and Redox Noninnocent Ligand. *J. Am. Chem. Soc.* **2017**, *139*, 6110– 6113, DOI: 10.1021/jacs.7b03070
34. Dauth, A.; Gellrich, U.; Diskin-Posner, Y.; Ben-David, Y.; Milstein, D. The ferraquinone–ferrahydroquinone couple: combining quinonic and metal-based reactivity. *J. Am. Chem. Soc.* **2017**, *139*, 2799– 2807, DOI: 10.1021/jacs.6b13050
35. Rosenkoetter, K. E.; Wojnar, M. K.; Charette, B. J.; Ziller, J. W.; Heyduk, A. F. Hydrogen-atom noninnocence of a tridentate [SNS] pincer ligand. *Inorg. Chem.* **2018**, *57*, 9728– 9737, DOI: 10.1021/acs.inorgchem.8b00618
36. Ward, M. B.; Scheitler, A.; Yu, M.; Senft, L.; Zillmann, A. S.; Gorden, J. D.; Schwartz, D. D.; Ivanović-Burmazović, D. D.; Goldsmith, C. R. Superoxide dismutase activity enabled by a redox-active ligand rather than metal. *Nat. Chem.* **2018**, *10*, 1207– 1212, DOI: 10.1038/s41557-018-0137-1
37. Drummond, M. J.; Ford, C. L.; Gray, D. L.; Popescu, C. V.; Fout, A. R. Radical Rebound Hydroxylation Versus H-Atom Transfer in Non-Heme Iron(III)-Hydroxo Complexes: Reactivity and Structural Differentiation. *J. Am. Chem. Soc.* **2019**, *141*, 6639– 6650, DOI: 10.1021/jacs.9b01516
38. Purse, B. W.; Tran, L.-H.; Piera, J.; Åkermark, B.; Bäckvall, J.-E. Bäckvall, Synthesis of New Hybrid Hydroquinone/Cobalt Schiff Base Catalysts: Efficient Electron-Transfer Mediators in Aerobic Oxidation. *Chem. – Eur. J.* **2008**, *14*, 7500– 7503, DOI: 10.1002/chem.200800657
39. Myers, T. W.; Berben, L. A. Aluminium–ligand cooperation promotes selective dehydrogenation of formic acid to H₂ and CO₂. *Chem. Sci.* **2014**, *5*, 2771– 2777, DOI: 10.1039/C4SC01035C
40. Henthorn, J. T.; Lin, S.; Agapie, T. Combination of Redox-Active Ligand and Lewis Acid for Dioxygen Reduction with π -Bound Molybdenum–Quinonoid Complexes. *J. Am. Chem. Soc.* **2015**, *137*, 1458– 1464, DOI: 10.1021/ja5100405
41. Lagaditis, P. O.; Schluschaß, B.; Demeshko, S.; Würtele, C.; Schneider, S. Square-Planar Cobalt (III) Pincer Complex. *Inorg. Chem.* **2016**, *55*, 4529– 4536, DOI: 10.1021/acs.inorgchem.6b00369
42. Schneck, F.; Finger, M.; Tromp, M.; Schneider, S. Chemical Non-Innocence of an Aliphatic PNP Pincer Ligand. *Chem. – Eur. J.* **2017**, *23*, 33– 37, DOI: 10.1002/chem.201604407
43. Lindley, B. M.; Bruch, Q. J.; White, P. S.; Hasanayn, F.; Miller, A. J. M. Ammonia Synthesis from a Pincer Ruthenium Nitride via Metal–Ligand Cooperative Proton-Coupled Electron Transfer. *J. Am. Chem. Soc.* **2017**, *139*, 5305– 5308, DOI: 10.1021/jacs.7b01323
44. Pramanick, R.; Bhattacharjee, R.; Sengupta, D.; Datta, A.; Goswami, S. An azoaromatic ligand as four electron four proton reservoir: catalytic dehydrogenation of alcohols by its zinc (II) complex. *Inorg. Chem.* **2018**, *57*, 6816– 6824, DOI: 10.1021/acs.inorgchem.8b00034
45. Jain, R.; Mamun, A. A.; Buchanan, R. M.; Kozłowski, P. M.; Grapperhaus, C. A. Ligand-assisted metal-centered electrocatalytic hydrogen evolution upon reduction of a bis

- (thiosemicarbazonato) Ni (II) complex. *Inorg. Chem.* **2018**, *57*, 13486–13493, DOI: 10.1021/acs.inorgchem.8b02110
46. Sherbow, T. J.; Thompson, E. J.; Arnold, A.; Saylor, R. I.; Britt, R. D.; Berben, L. A. Electrochemical Reduction of N₂ to NH₃ at Low Potential by a Molecular Aluminum Complex. *Chem. – Eur. J* **2019**, *25*, 454–458, DOI: 10.1002/chem.201804454
47. McNeece, A. J.; Jesse, K. A.; Filatov, A. S.; Schneider, J. E.; Anderson, J. S., Catalytic hydrogenation enabled by ligand-based storage of hydrogen. *Chem. Comm.* **2021**, *57*, 3869-3872.
48. McNeece, A. J.; Jesse, K. A.; Xie, J.; Filatov, A. S.; Anderson, J. S., Generation and Oxidative Reactivity of a Ni(II) Superoxo Complex via Ligand-Based Redox Non-Innocence. *J. Am. Chem. Soc.* **2020**, *142*, 10824-10832.
49. Beyene, B. B.; Hung, C.-H., Recent progress on metalloporphyrin-based hydrogen evolution catalysis. *Coord. Chem. Rev.* **2020**, *410*, 213234.
50. Canaguier, S.; Artero, V.; Fontecave, M., Modelling NiFe hydrogenases: nickel-based electrocatalysts for hydrogen production. *Dalton Trans.* **2008**, 315-325.
51. Dressel, J.M.; Cook, E.N.; Hooe, S.L.; Moreno, J.J.; Dickie, D.A.; Machan, C.W., Electrocatalytic hydrogen evolution reaction by a Ni(N₂O₂) complex based on 2,2'-bipyridine. *Inorg. Chem. Front.* **2023**, *10*, 972-978.
52. Fang, M.; Engelhard, M. H.; Zhu, Z.; Helm, M. L.; Roberts, J.A.S., Electrodeposition from acidic solutions of Nickel bis(benzenedithiolate) produces a hydrogen evolving Ni-S film on glassy carbon. *ACS Catal.* **2014**, *4*, 90-98.
53. Han, Z.; Shen, L.; Brennessel, W. W.; Holland, P. L.; Eisenberg, R., Nickel Pyridinethiolate Complexes as Catalysts for the Light-Driven Production of Hydrogen from Aqueous Solutions in Noble-Metal-Free Systems. *J. Am. Chem. Soc.* **2013**, *135*, 14659-14669.
54. Helm, M. L.; Stewart, M. P.; Bullock, R. M.; DuBois, M. R.; DuBois, D. L., A Synthetic Nickel Electrocatalyst with a Turnover Frequency Above 100,000 s⁻¹ for H₂ Production. *Science* **2011**, *333*, 863-866.
55. Jacques, P.; Artero, V.; Pecaut, J.; Fontecave, M., Cobalt and nickel diimine-dioxime complexes as molecular electrocatalysts for hydrogen evolution with low overvoltages. *Proc. Natl. Acad. Sci.* **2009**, *106*, 20627-20632.
56. Khrizanforova, V. V.; Fayzullin, R. R.; Musina, E. I.; Karasik, A. A.; Budnikova, Y. H., Electrochemical and catalytic properties of nickel(II) complexes with bis(imino)acenaphthene and diazadiphosphacyclooctane ligands. *Mendeleev Commun.* **2020**, *30*, 302-304.
57. Martin, D. J.; McCarthy, B. D.; Donley, C. L.; Dempsey, J. L., Electrochemical hydrogenation of a homogeneous nickel complex to form a surface adsorbed hydrogen-evolving species. *Chem. Comm.* **2015**, *51*, 5290-5293.
58. Pantani, O.; Anxolabéhère-Mallart, E.; Aukauloo, A.; Millet, P., Electroactivity of cobalt and nickel glyoximes with regard to the electro-reduction of protons into molecular hydrogen in acidic media. *Electrochem. Commun.* **2007**, *9*, 54-58.
59. Rao, H.; Yu, W.-Q.; Zheng, H.-Q.; Bonin, J.; Fan, Y.-T.; Hou, H.-W., Highly efficient photocatalytic hydrogen evolution from nickel quinolinethiolate complexes under visible light irradiation. *J. Power Sources* **2016**, *324*, 253-260.
60. Shotonwa, I. O.; Ejeromedoghene, O.; Adesoji, A. O.; Adewuyi, S., Electrochemistry and electrocatalysis of H₂ generation using hexacoordinated nickel—based complexes. *Catal. Comm.* **2023**, *179*, 106680.
61. Newcomb, M., Radical Kinetics and Clocks. In *Encyclopedia of Radicals in Chemistry, Biology and Materials*, 2012.
62. Stoll, S.; Schweiger, A. EasySpin, a comprehensive software package for spectral simulation and analysis in EPR. *J. Magn. Reson.* **2006**, *178*, 42–55.
63. Krause, L.; Herbst-Irmer, R.; Sheldrick, G. M.; Stalke, D. Comparison of Silver and Molybdenum Microfocus X-Ray Sources for Single-Crystal Structure Determination. *J. Appl. Crystallogr.* **2015**, *48*, 3–10.
64. Sheldrick, G. M. SHELXT - Integrated Space-Group and Crystal-Structure Determination. *Acta Crystallogr., Sect. A: Found. Adv.* **2015**, *71*, 3– 8.
65. Dolomanov, O. V.; Bourhis, L. J.; Gildea, R. J.; Howard, J. A. K.; Puschmann, H. OLEX2: A Complete Structure Solution, Refinement and Analysis Program. *J. Appl. Crystallogr.* **2009**, *42*, 339– 341.
66. Sheldrick, G. M. Crystal Structure Refinement with SHELXL. *Acta Crystallogr., Sect. C: Struct. Chem.* **2015**, *71*, 3– 8.
67. Neese, F. The ORCA program system. *WIREs Comput. Mol. Sci.* **2012**, *2*, 73-78.